

Study of maximal bipartite entanglement and robustness in resonating-valence-bond states

Muzaffar Q. Lone¹ and Sudhakar Yarlagadda^{1,2}

¹*TCMP Div. and* ²*CAMCS*

*1/AF Salt Lake, Saha Institute of Nuclear physics,
Calcutta, India -700064*

We study maximal bipartite entanglement in valence-bond states and show that the average bipartite entanglement E_v^2 , between a sub-system of two spins and the rest of the system, can be maximized through a homogenized superposition of the valence-bond states. Our derived maximal E_v^2 rapidly increases with system size and saturates at its maximum allowed value. We also demonstrate that our maximal E_v^2 states are ground states of an infinite range Heisenberg model (IRHM) and represent a new class of resonating-valence-bond (RVB) states. The entangled RVB states produced from our IRHM are robust against interaction of spins with both local and global phonons and represent a new class of decoherence free states.

PACS numbers: 03.67.Mn, 03.65.Yz, 03.67.Bg, 05.50.+q

I. INTRODUCTION.

Quantum entanglement, a manifestation of non-locality, is a precious resource for quantum computation and quantum information [1] and signifies correlations in many-body systems. Quantum algorithms that would significantly accelerate a classical computation must rely on highly entangled states since slightly entangled states can be simulated efficiently on a classical computer [2]. The strength of correlations of fluctuations of observables (such as density, magnetization, etc.) in a many-body system is a reflection of the degree of entanglement (for pure states) [3]. Thus, characterization of multi-particle entanglement and production of maximal/high multi-qubit entanglement is vital for quantum computational studies and for mutual enrichment of quantum information and many-body condensed matter physics.

Intensive work on entanglement during the past decade has led to the proposal of numerous measures of entanglement [4, 5]. While two-party entanglement is quite well understood, entanglement in a multi-party system is an area of immense current interest [6–13]. In the quest for maximally entangled states, so far only few-qubit maximally entangled states such as two-qubit Bell states, three-qubit Greenberger-Horne-Zeilinger (GHZ) states, and four-qubit Higuchi-Sudbery (HS) states [14] have been clearly identified. It would be of considerable interest to generate these maximally entangled states as the ground states of a physically realizable spin model. While the GHZ states could be obtained as the ground state of an anisotropic Heisenberg model [15], maximally entangled four-qubit and five-qubit states could be obtained only as excited states [16].

Decoherence is one of the main obstacles for the preparation, observation, and implementation of multi-qubit entangled states. Since coupling to the environment and the concomitant entanglement fragility are ubiquitous [1, 17], it is imperative that progress be made in understanding decoherence as well. In

the past decoherence-free-subspace (DFS) [18, 19] has been shown to exist in the Hilbert space of a model where all qubits of the quantum system are coupled to a common environment with equal strength. This situation manifests when the distance between the qubits is negligible compared to the correlation length of the environment. If the dynamic symmetry of the system-environment interaction selects a set of orthonormal basis vectors (of the reduced Hilbert space) that is unaffected by environmental interaction, then such a subspace is called a DFS. An important application of decoherence free subspaces lies in developing quantum error correcting codes [20, 21]. These subspaces prevent the loss of information due to destructive environmental interactions and thus circumvent the need for stabilization methods for quantum computation and quantum information. Decoherence free states have also been shown to be useful for quantum communication between parties without a common reference frame [22–26].

RVB states have provided interesting insights for understanding strongly correlated phenomena such as physics of high T_c cuprates [27, 28], superconductivity in organic solids [29], insulator-superconductor transition in boron-doped diamond [30], etc. Furthermore, RVB states have also been proposed as robust basis states for topological quantum computation [31]. The multi-particle entanglement has also been investigated in RVB states that were proposed as states close in energy to the ground state of the Heisenberg Hamiltonian [32–34]. However, there has been no explicit construction of RVB states that would represent maximally entangled valence bond states. In this paper we construct a new class of RVB states that are ground states of IRHM, that have high E_v^2 entanglement, and are decoherence free. Our IRHM Hamiltonian couples to an environment that distinguishes between the qubits unlike the case considered in Ref. 19. We believe that an improved understanding of the entanglement and decoherence properties of RVB states will enable their implementation for quantum com-

putation and quantum information purposes.

The remainder of this paper is organized as follows. In section II, we introduce entanglement entropy and demonstrate explicitly that isotropy and homogeneity maximizes entanglement E_v^2 between two spins and the rest of the system in the two limits of even- N -qubits, i.e., for $N = 4$ and $N \rightarrow \infty$. For intermediate even- N -spin states, our proposed entangled states are only shown to maximize E_v^2 among valence-bond states. In section III, from the ground states of our IRHM, we construct explicitly states with maximal E_v^2 entanglement among valence-bond states and show that these states form a special class of RVB states. Next, in section IV, we analyze the robustness of this special class of entangled states. We show that our IRHM Hamiltonian, even upon inclusion of both local and global optical phonons that are coupled to spins, produces ground states that are decoherence free. Lastly, in the final section V, we conclude after commenting on the physical realizability of our proposed high E_v^2 entangled states.

II. ENTANGLEMENT FOR TWO-QUBIT REDUCED DENSITY MATRIX IN ISOTROPIC SYSTEM.

For a bipartite system AB in a pure state, von Neumann entropy E_v measures the entanglement between the subsystems A and B. From the reduced density matrices $\rho_A \equiv \text{tr}_B \rho^{AB}$ and $\rho_B \equiv \text{tr}_A \rho^{AB}$ obtained from the pure state ρ^{AB} , we obtain

$$\begin{aligned} E_v(\rho_A) &= -\text{tr}(\rho_A \log_2 \rho_A) \\ &= -\text{tr}(\rho_B \log_2 \rho_B) = E_v(\rho_B). \end{aligned} \quad (1)$$

Using the basis $|\downarrow\rangle, |\uparrow\rangle$, and $S^i = \frac{1}{2}\sigma^i$, the single qubit density matrix can be written as [35]

$$\rho_i = \begin{bmatrix} \frac{1}{2} - \langle S_i^z \rangle & \langle S_i^+ \rangle \\ \langle S_i^- \rangle & \frac{1}{2} + \langle S_i^z \rangle \end{bmatrix}. \quad (2)$$

Throughout this paper, we consider only states $|\Psi\rangle$ that are eigenstates of the z-component of the total spin operator (S_{Total}^z) with eigenvalue S_T^z ; furthermore, we focus on only isotropic states. It then follows that, $\langle S_i^z \rangle = 0$ and $\langle S_i^+ \rangle = 0$ leading to the single-qubit density matrix to be maximally mixed and thus maximizing entanglement $E_v(\rho_i)$. On realizing that $\langle S_i^z \rangle = 0$, we obtain the following expression for the two-qubit reduced density matrix [35]:

$$\rho_{ij} = \begin{bmatrix} \frac{1}{4} + \langle S_i^z S_j^z \rangle & 0 & 0 & 0 \\ 0 & \frac{1}{4} - \langle S_i^z S_j^z \rangle & \langle S_i^+ S_j^- \rangle & 0 \\ 0 & \langle S_i^- S_j^+ \rangle & \frac{1}{4} - \langle S_i^z S_j^z \rangle & 0 \\ 0 & 0 & 0 & \frac{1}{4} + \langle S_i^z S_j^z \rangle \\ \cdot & & & \end{bmatrix}. \quad (3)$$

Here, isotropy implies $0.5\langle S_i^- S_j^+ \rangle = 0.5\langle S_i^+ S_j^- \rangle = \langle S_i^x S_j^x \rangle = \langle S_i^y S_j^y \rangle = \langle S_i^z S_j^z \rangle$. Thus, the von Neumann

entropy $E_v(\rho_{ij})$ can be expressed as

$$\begin{aligned} E_v(\rho_{ij}) &= 2 - \frac{1}{4} [3(1 + 4\langle S_i^z S_j^z \rangle) \log_2(1 + 4\langle S_i^z S_j^z \rangle) \\ &\quad + (1 - 12\langle S_i^z S_j^z \rangle) \log_2(1 - 12\langle S_i^z S_j^z \rangle)]. \end{aligned} \quad (4)$$

For our states, $S_{Total}^z |\Psi\rangle = 0$ which implies that $\langle S_i^z \sum_j S_j^z \rangle = 0$, that is,

$$\sum_{j \neq i} \langle S_i^z S_j^z \rangle = -\langle S_i^z \rangle = -\frac{1}{4}. \quad (5)$$

We will now maximize the total entanglement entropy $\sum_{i,j \neq i} E_v(\rho_{ij})$ subject to the above constraint in Eq. (5). To this end, we will employ the method of Lagrange multipliers and define the Lagrange function Λ as follows:

$$\Lambda = \sum_{i,j \neq i} E_v(\rho_{ij}) - \sum_i \lambda_i \left(\sum_{j \neq i} \langle S_i^z S_j^z \rangle + \frac{1}{4} \right). \quad (6)$$

Then, setting $\frac{\partial \Lambda}{\partial \langle S_i^z S_m^z \rangle} = 0$ yields

$$\lambda_l = 3 \log_2 \left[\frac{(1 - 12\langle S_l^z S_m^z \rangle)}{(1 + 4\langle S_l^z S_m^z \rangle)} \right], \quad (7)$$

which implies that the optimal $\langle S_i^z S_j^z \rangle$ is independent of j for $j \neq i$. Consequently, it follows from Eq. (5) that $\sum_{i,j \neq i} E_v(\rho_{ij})$ is maximized when $\langle S_i^z S_j^z \rangle = -\frac{1}{4(N-1)}$, i.e., when the isotropic state is *homogeneous*. The average entanglement entropy between the subsystem of two spins and the rest of the system (of $N - 2$ spins) $E_v^2 \equiv [1/N(N-1)] \sum_{i,j \neq i} E_v(\rho_{ij})$ has a maximum value given by

$$\begin{aligned} E_{v,max}^2 &= -3 \left(\frac{1}{4} - \frac{1}{4(N-1)} \right) \log_2 \left(\frac{1}{4} - \frac{1}{4(N-1)} \right) \\ &\quad - \left(\frac{1}{4} + \frac{3}{4(N-1)} \right) \log_2 \left(\frac{1}{4} + \frac{3}{4(N-1)} \right). \end{aligned} \quad (8)$$

It is interesting to note that for $N \rightarrow \infty$, the above expression yields $E_v^2 \rightarrow 2$. In fact, E_v^2 approaches the maximum possible value 2 quite rapidly as can be seen from Fig. 1. Next, we observe that for $N = 4$, our expression for $E_{v,max}^2$ in Eq. (8) yields the same entanglement entropy value $1 + 0.5 \log_2 3$ as that obtained for the four-qubit maximally entangled HS state [10, 14]. Furthermore, our approach explains why all the pairs in the HS state give the same entanglement value. Contrastingly, for the isotropic ground state, in the case of a Heisenberg chain with nearest-neighbor interaction, for four spins the entanglement entropy $E_v^2 = 1.21$ (with $\langle S_i^z S_j^z \rangle = -0.5/3$) while for an infinite chain the von Neumann entropy $E_v^2 = 1.37$ (with $\langle S_i^z S_j^z \rangle \approx -0.443/3$) both of which are far less than our maximal E_v^2 values above. It is of interest to note that, when $N = 4$ or $N \rightarrow \infty$, the maximal values of E_v^2 for isotropic systems are the same as the maximal E_v^2 values for general systems (i.e., systems that can be either isotropic or non-isotropic).

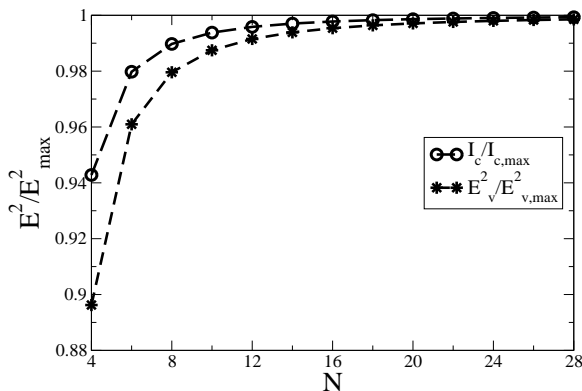


FIG. 1. Normalized entanglement E^2/E_{\max}^2 , for two-qubit reduced density matrix, measured by (a) von Neumann entropy ($E_v^2/E_{v,\max}^2$) and (b) i-concurrence ($I_c/I_{c,\max}$), for N -qubit valence-bond systems.

We also note that homogeneity, under the constraint of Eq. (5), maximizes the i-concurrence (I_c) [36] given by

$$I_c = \frac{2}{N(N-1)} \sum_{i,j>i} \sqrt{2[1 - \text{Tr}(\rho_{ij}^2)]}. \quad (9)$$

As shown in Fig. 1, I_c also monotonically increases with system size. Although we considered von Neumann entropy and i-concurrence as entanglement measures, our homogeneous states should also maximize other measures of entanglement for ρ_{ij} in valence-bond systems.

III. MULTI-QUBIT ENTANGLED STATES.

A. Highly entangled ground states of IRHM

We will now demonstrate that ground states of the IRHM Hamiltonian

$$H_{\text{IRHM}} = J \sum_{i,j>i} \vec{S}_i \cdot \vec{S}_j = \frac{J}{2} \left[\left(\sum_i \vec{S}_i \right)^2 - \left(\sum_i \vec{S}_i^2 \right) \right], \quad (10)$$

will produce the same amount of entanglement as given by Eq. (8). We note that H_{IRHM} commutes with both S_{Total}^z and $\left(\sum_i \vec{S}_i \right)^2$ ($\equiv S_{\text{Total}}^2$). In Eq. (10), it is understood that $J = J^*/(N-1)$ (where J^* is a finite quantity) so that the energy per site remains finite as $N \rightarrow \infty$. The eigenstates of H_{IRHM} correspond to eigenenergies

$$E_{S_T} = \frac{J}{2} \left[S_T(S_T + 1) - \frac{3N}{4} \right], \quad (11)$$

where S_T is the total spin eigenvalue. The ground state corresponds to $S_T = 0$ which is rotationally invariant and also implies that $S_T^z = 0$. Thus for a homogenized linear combination of the $S_T = 0$ states of H_{IRHM} , the

entanglement is given by Eq. (8). It is important to note that, while all possible $S_T = 0$ states are ground states of IRHM, for some Hamiltonians only some of the possible $S_T = 0$ states are ground states. For instance, for the nearest-neighbor antiferromagnetic Heisenberg Hamiltonian or for the Majumdar-Ghosh model Hamiltonian [37] only some of the possible $S_T = 0$ states are ground states and consequently (for these systems) it is not possible to construct a homogenized linear combination of $S_T = 0$ ground states that produces maximal possible entanglement $E_{v,\max}^2$ given by Eq. (8).

We will now proceed to construct entangled states for N spins that maximize E_v^2 . We first note that there are $(N-1)!!$ eigenstates with $S_T = 0$ for the Hamiltonian of Eq. (10). Each of the $S_T = 0$ states is a product of $N/2$ two-spin singlet states of the form $|\uparrow\downarrow\rangle - |\downarrow\uparrow\rangle$ (with no pair of singlets sharing a spin). Of these $(N-1)!!$ product combinations with $S_T = 0$, only ${}^N C_{\frac{N}{2}} - {}^N C_{\frac{N}{2}-1} = N!/[(N/2)!(N/2+1)!]$ products are linearly independent. A particular set of linearly independent $S_T = 0$ states are the Rumer states [38, 39] which are made up of non-crossing singlets. For $N = 6$, the Rumer states are the 5 diagrams with non-crossing singlets shown in Fig. 2.

For $N = 4$ spins, two linearly independent $S_T = 0$ eigenstates are $|\Phi_{12}^{S_{12}=0}\rangle \otimes |\Phi_{34}^{S_{34}=0}\rangle$ and $|\Phi_{14}^{S_{14}=0}\rangle \otimes |\Phi_{23}^{S_{23}=0}\rangle$ where $|\Phi_{ij}^{S_{ij}=0}\rangle$ is a two-spin singlet state for spins at sites i and j with S_{ij} being the total spin of S_i and S_j . It is worth noting that

$$|\Phi_{13}^{S_{13}=0}\rangle \otimes |\Phi_{24}^{S_{24}=0}\rangle = |\Phi_{12}^{S_{12}=0}\rangle \otimes |\Phi_{34}^{S_{34}=0}\rangle + |\Phi_{14}^{S_{14}=0}\rangle \otimes |\Phi_{23}^{S_{23}=0}\rangle. \quad (12)$$

Using the above relation one can establish that there are only ${}^N C_{\frac{N}{2}} - {}^N C_{\frac{N}{2}-1}$ linearly independent $S_T = 0$ states. Furthermore, we also observe that

$$[\vec{S}_1 \cdot \vec{S}_3 + \vec{S}_2 \cdot \vec{S}_4 + \vec{S}_1 \cdot \vec{S}_4 + \vec{S}_2 \cdot \vec{S}_3] |\Phi_{12}^{S_{12}=0}\rangle \otimes |\Phi_{34}^{S_{34}=0}\rangle = 0,$$

using which it can be shown that any $S_T = 0$ state made up of $N/2$ singlets will be an eigenstate of Eq. (10).

Now, while the two symmetry broken $S_T = 0$ singlet states [on the right hand side of Eq. (12)] are isotropic, they are not homogeneous. To make our entangled state homogeneous, we construct the following state that has the symmetry that $\langle S_i^\eta S_j^\eta \rangle$ is the same ($= -1/12$) for all pairs i and j and any $\eta = (x, y, z)$:

$$\begin{aligned} & \omega_3(|\Phi_{12}^{S_{12}=0}\rangle \otimes |\Phi_{34}^{S_{34}=0}\rangle) + \omega_3^2(|\Phi_{14}^{S_{14}=0}\rangle \otimes |\Phi_{23}^{S_{23}=0}\rangle) \\ &= \frac{1}{\sqrt{6}} (|\uparrow\downarrow\uparrow\downarrow\rangle + |\downarrow\uparrow\downarrow\uparrow\rangle) + \omega_3 (|\uparrow\downarrow\downarrow\uparrow\rangle + |\downarrow\uparrow\uparrow\downarrow\rangle) \\ & \quad + \omega_3^2 (|\uparrow\uparrow\downarrow\downarrow\rangle + |\downarrow\downarrow\uparrow\uparrow\rangle) \\ & \equiv |\Psi_{\text{HS}}\rangle, \end{aligned} \quad (13)$$

where ω_3 's are cube roots of unity. The above $|\Psi_{\text{HS}}\rangle$ state is the maximally entangled four-qubit HS state studied by many authors [10, 13, 14, 16]. However, it has not been shown earlier that $|\Psi_{\text{HS}}\rangle$ can be expressed as a superposition of $S_T = 0$ states. Importantly, the

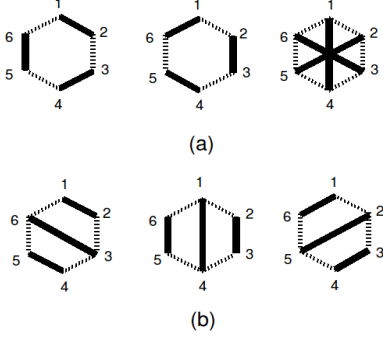


FIG. 2. Homogenized linear combination of the $S_T = 0$ states in both (a) and (b) give the same maximal entanglement for six qubits.

half-filled large U/t Hubbard model on a regular tetrahedron yields the above two broken-symmetry $S_T = 0$ states as ground states from which the HS-state can be constructed. In previous reported works [40, 41], although the authors studied entanglement in the model $H = J\sum_{i,j=1,2,3,4}\vec{S}_i\cdot\vec{S}_j$, they did not point out that the maximally entangled HS state is a ground state of the

model.

The above strategy of constructing homogeneous and maximal E_v^2 states from isotropic four-qubit states can be extended to the six-qubit case as well using the $S_T = 0$ ground states of H_{IRHM} shown in the six diagrams of Fig. 2. The entanglement E_v^2 for the six-qubit states is maximized by taking suitable resonance hybrids of the diagrams shown in Figs. 2 (a) or (b). These resonance states homogenize the ground state in the sense mentioned above (i.e., produce site independent correlation functions $\langle S_i^\eta S_j^\eta \rangle = -1/20$):

$$\begin{aligned} |\Psi_6^a\rangle &= \omega_4(|\Phi_{12}^{S_{12}=0}\rangle \otimes |\Phi_{34}^{S_{34}=0}\rangle \otimes |\Phi_{65}^{S_{65}=0}\rangle) \\ &+ \omega_4^2(|\Phi_{61}^{S_{61}=0}\rangle \otimes |\Phi_{23}^{S_{23}=0}\rangle \otimes |\Phi_{45}^{S_{45}=0}\rangle) \\ &+ \omega_4^3(|\Phi_{14}^{S_{14}=0}\rangle \otimes |\Phi_{25}^{S_{25}=0}\rangle \otimes |\Phi_{36}^{S_{36}=0}\rangle), \end{aligned} \quad (14)$$

and

$$\begin{aligned} |\Psi_6^b\rangle &= \omega_4(|\Phi_{12}^{S_{12}=0}\rangle \otimes |\Phi_{36}^{S_{36}=0}\rangle \otimes |\Phi_{45}^{S_{45}=0}\rangle) \\ &+ \omega_4^2(|\Phi_{23}^{S_{23}=0}\rangle \otimes |\Phi_{14}^{S_{14}=0}\rangle \otimes |\Phi_{56}^{S_{56}=0}\rangle) \\ &+ \omega_4^3(|\Phi_{16}^{S_{16}=0}\rangle \otimes |\Phi_{25}^{S_{25}=0}\rangle \otimes |\Phi_{34}^{S_{34}=0}\rangle), \end{aligned} \quad (15)$$

which can be rewritten as

$$\begin{aligned} |\Psi_6^a\rangle &= \frac{1}{\sqrt{20}}[(|\uparrow\uparrow\uparrow\downarrow\uparrow\downarrow\rangle - |\downarrow\uparrow\downarrow\uparrow\uparrow\downarrow\rangle) + \omega_4(|\uparrow\downarrow\uparrow\downarrow\uparrow\uparrow\rangle + |\uparrow\downarrow\downarrow\uparrow\uparrow\downarrow\rangle + |\downarrow\uparrow\uparrow\downarrow\uparrow\downarrow\rangle - |\uparrow\downarrow\downarrow\uparrow\uparrow\rangle - |\uparrow\downarrow\uparrow\downarrow\uparrow\rangle - |\downarrow\uparrow\downarrow\uparrow\uparrow\rangle) \\ &+ \omega_4^2(|\uparrow\uparrow\downarrow\uparrow\downarrow\rangle + |\uparrow\downarrow\uparrow\uparrow\downarrow\rangle + |\downarrow\downarrow\uparrow\uparrow\uparrow\rangle - |\uparrow\uparrow\downarrow\uparrow\downarrow\rangle - |\downarrow\uparrow\downarrow\uparrow\uparrow\rangle - |\downarrow\downarrow\uparrow\uparrow\uparrow\rangle) \\ &+ \omega_4^3(|\uparrow\uparrow\uparrow\downarrow\downarrow\rangle + |\uparrow\downarrow\downarrow\uparrow\uparrow\rangle + |\downarrow\downarrow\uparrow\uparrow\downarrow\rangle - |\uparrow\uparrow\downarrow\uparrow\uparrow\rangle - |\uparrow\uparrow\uparrow\downarrow\downarrow\rangle - |\downarrow\downarrow\uparrow\uparrow\uparrow\rangle)], \end{aligned} \quad (16)$$

and

$$\begin{aligned} |\Psi_6^b\rangle &= \frac{1}{\sqrt{20}}[(|\uparrow\downarrow\uparrow\downarrow\uparrow\downarrow\rangle - |\downarrow\uparrow\downarrow\uparrow\uparrow\downarrow\rangle) + \omega_4(|\uparrow\downarrow\uparrow\uparrow\downarrow\rangle + |\uparrow\downarrow\downarrow\uparrow\uparrow\rangle + |\downarrow\uparrow\uparrow\downarrow\uparrow\rangle - |\uparrow\downarrow\uparrow\uparrow\rangle - |\downarrow\uparrow\uparrow\downarrow\rangle - |\downarrow\uparrow\downarrow\uparrow\uparrow\rangle) \\ &+ \omega_4^2(|\uparrow\uparrow\downarrow\uparrow\downarrow\rangle + |\uparrow\downarrow\uparrow\downarrow\uparrow\rangle + |\downarrow\downarrow\uparrow\uparrow\downarrow\rangle - |\uparrow\uparrow\downarrow\uparrow\uparrow\rangle - |\downarrow\uparrow\downarrow\uparrow\downarrow\rangle - |\downarrow\downarrow\uparrow\uparrow\uparrow\rangle) \\ &+ \omega_4^3(|\uparrow\uparrow\uparrow\downarrow\downarrow\rangle + |\downarrow\downarrow\uparrow\uparrow\uparrow\rangle + |\uparrow\downarrow\uparrow\uparrow\downarrow\rangle - |\uparrow\uparrow\downarrow\uparrow\downarrow\rangle - |\downarrow\uparrow\downarrow\uparrow\uparrow\rangle - |\downarrow\downarrow\uparrow\uparrow\uparrow\rangle)], \end{aligned} \quad (17)$$

where ω_4 's are fourth roots of unity. The von Neumann entropy E_v^2 , for two-qubit reduced density matrix obtained from $|\Psi_6^a\rangle$, $(|\Psi_6^a\rangle)^*$, $|\Psi_6^b\rangle$, or $(|\Psi_6^b\rangle)^*$, is 1.921964 which is the same as $E_{v,max}^2$ proposed by our general formula in Eq. (8). The conjecture made by Brown *et al.* [13] that the multi-qubit maximally entangled states always have their reduced single qubit density matrix maximally mixed is satisfied by our states $|\Psi_6\rangle$. It should be noted that the highly entangled six-qubit state reported in Ref. [10], although yields a higher entanglement, is not an eigenstate of the S_{Total}^z operator.

Cabello [42] has constructed supersinglets of four and six qubits which are decoherence free. It is interesting to note that they form the ground states of our IRHM Hamiltonian. However, the average two particle von Neu-

mann entanglement entropy E_v^2 for these supersinglets is less than the entanglement for our states constructed above. In the case of the four qubit supersinglet state $|\mathcal{S}_4^{(2)}\rangle$, the entanglement entropies for all possible bipartitions are given by $E_v(\rho_{12}) = E_v(\rho_{34}) = 1.5849$, $E_v(\rho_{13}) = E_v(\rho_{24}) = 1.2075$, $E_v(\rho_{14}) = E_v(\rho_{23}) = 1.2075$ which together yield the average two particle entropy value 1.3333, i.e., a quantity clearly smaller than the von Neumann entropy $E_v^2 = 1 + 0.5\log_2 3 \approx 1.79248$ obtained for the four-qubit maximally entangled HS state. In the six qubit supersinglet $|\mathcal{S}_6^{(2)}\rangle$ case, the various bipartitions produce the average entropy $E_v^2 = 1.657996$ which is noticeably smaller than the entropy value $E_{v,max}^2 = 1.921964$ obtained for our six qubit en-

tangled states.

On the issue of how many maximal E_v^2 states are possible for N qubit systems, we would like to say that it cannot exceed the total number of linearly independent $S_T = 0$ states (i.e., the total number of Rumer states). As regards existence of homogeneous states for $N \geq 8$ qubit systems, we provide arguments in Appendix A.

B. Resonating-valence-bond picture

The construction of our entangled maximal E_v^2 states from the ground states of IRHM can be visualized by using a RVB picture. Our maximal E_v^2 states can be regarded as a new class of RVB states made of homogenized superposition of isotropic $S_T = 0$ valence bond states. We will now compare the entanglement properties of our RVB states and the general RVB states $|\Psi\rangle_{\text{rvb}}$ of Ref. 33 given below:

$$|\Psi\rangle_{\text{rvb}} = \sum_{\substack{i_\alpha \in A \\ j_\beta \in B}} f(i_1, \dots, i_M, j_1, \dots, j_M) |(i_1, j_1) \dots (i_M, j_M)\rangle,$$

where M represents the number of sites in each sub-lattice and f is assumed to be isotropic over the lattice. Also, $|(i_k, j_k)\rangle \equiv \frac{1}{\sqrt{2}}(|\frac{1}{2}\rangle_{i_k} |-\frac{1}{2}\rangle_{j_k} - |-\frac{1}{2}\rangle_{i_k} |\frac{1}{2}\rangle_{j_k})$ denotes the singlet dimer connecting a site in sub-lattice A with a site in sub-lattice B . The valence bond basis (used for the above RVB state $|\Psi\rangle_{\text{rvb}}$) form an over complete set while our RVB states are constructed from a complete set of ${}^N C_{\frac{N}{2}} - {}^N C_{\frac{N}{2}-1}$ states.

The rotational invariance of the two qubit reduced density matrix of the RVB states allows us to write them in the form of a Werner state:

$$\rho_w(p) = p|(ij)\rangle\langle ij| + \frac{1-p}{4}I_4, \quad (18)$$

where for $1/3 < p \leq 1$ the Werner state has the spins at i and j entangled with each other. For the special case of the ‘‘RVB gas’’ for the $|\Psi\rangle_{\text{rvb}}$ state, where f is a constant (corresponding to equal amplitude superposition of all bipartite valence bond coverings), one gets the exact result $p = 1/3 + 2/(3N)$ which implies that all finite size systems have a non-zero tangle (or entanglement) between the two sites [33]. Next, for the ‘‘RVB liquid’’ case (involving equal amplitude superposition of all nearest-neighbor singlet valence bond coverings of a lattice), Monte Carlo calculations extrapolated to the thermodynamic limit yield $p = 0.3946(3) > 1/3$ [33], i.e., a non-zero tangle between the two sites [43]. In contrast, our maximal E_v^2 RVB states yield zero entanglement between the two spins for all system sizes as demonstrated below. It has been shown that the $SU(2)$ symmetry of the RVB states ensures that the two-spin correlation function and the parameter p of the Werner state are related as

$$\langle \Psi | \vec{S}_i \cdot \vec{S}_j | \Psi \rangle = -\frac{3}{4}p. \quad (19)$$

Then, since our RVB states produce

$$\langle S_i^x S_j^x \rangle = \langle S_i^y S_j^y \rangle = \langle S_i^z S_j^z \rangle = \frac{-1}{4(N-1)}, \quad (20)$$

it follows that $p = \frac{1}{N-1}$ and thus for all even $N \geq 4$ systems we get zero entanglement between the two sites. Lastly, based on Ref. 33, we find that the monogamy argument yields the bound $p \leq 1/3 + 2/(3\sqrt{N-1})$ while the quantum telecloning argument produces the bound $p \leq 1/3 + 2/[3(N-1)]$. Compared to our exact value of $p = 1/(N-1)$, both these bounds are weaker bounds (i.e., show zero two-site entanglement with certainty only in the thermodynamic limit). Thus (among various RVB states) we see that our entangled high E_v^2 RVB states, while producing maximum entanglement between a pair and the rest of the system, yield zero entanglement among the two spins of the pair.

We will now remark on the entanglement of any set of n (> 2) sites with the rest of the system. The valence bond entanglement entropy picture of Alet *et al.* in Ref. 34 uses the number of valence bond two-spin singlets shared by the two subsystems as a measure of their entanglement with each other. Thus, our ‘homogenized’ RVB states, will always have shared bonds between the two subsystems and thus show high bipartite entanglement. However, exact quantitative analysis needs to be carried out. Extending our approach to deriving the n -qubit reduced density matrix in terms of n -particle correlation functions (when $n > 2$) and obtaining entanglement expressions and wavefunctions corresponding to maximal bipartite entanglement is a non-trivial exercise and is left for future studies.

IV. ROBUST ENTANGLEMENT.

The real quantum computer will not be free from noise and thus the entangled states have a tendency to undergo decoherence. However if the entangled state, in the presence of potentially decoherence producing interactions, still remains entangled we call such a state robust otherwise it is fragile. We will now present two extreme cases of system-environment interaction scenarios where the ground states of our IRHM as well as the highly entangled RVB states (that we construct from the ground states) are decoherence free.

A. Decoherence due to local optical phonons

To study decoherence due to phonons, we consider interaction with optical phonons such as would be encountered when considering a Hubbard model. The total Hamiltonian H_T is given by

$$H_T = H_{\text{IRHM}} + g\omega_0 \sum_i S_i^z (a_i^\dagger + a_i) + \omega_0 \sum_i a_i^\dagger a_i, \quad (21)$$

where a is the phonon destruction operator, ω_0 is the optical phonon frequency, and g is the coupling strength. Then, using the steps given in Appendix B, we obtain the following effective Hamiltonian H_e through second-order perturbation theory for strong coupling ($g > 1$) and non-adiabatic ($J/\omega_0 \leq 1$) conditions:

$$H_e = \sum_{i,j>i} [J_{\perp}(S_i^x S_j^x + S_i^y S_j^y) + J_{\parallel} S_i^z S_j^z] - g^2 \omega_0 \sum_i S_i^z, \quad (22)$$

where

$$J_{\perp} \equiv J e^{-g^2} - (N-2) f_1(g) \frac{J^2 e^{-2g^2}}{2\omega_0}, \quad (23)$$

$$J_{\parallel} \equiv J + [2f_1(g) + f_2(g)] \frac{J^2 e^{-2g^2}}{2\omega_0}, \quad (24)$$

with $f_1(g) \equiv \sum_{n=1}^{\infty} g^{2n}/(n!n)$ and $f_2(g) \equiv \sum_{n=1}^{\infty} \sum_{m=1}^{\infty} g^{2(n+m)}/[n!m!(n+m)]$. It is interesting to note that the eigenstates of the effective Hamiltonian H_e in Eq. (22) are identical to those of the original Hamiltonian H_{IRHM} in Eq. (10) because $[\sum_{i,j>i} (S_i^z S_j^z), H_{\text{IRHM}}] = 0$. Furthermore, even upon carrying out higher-order (i.e., beyond second-order) perturbation theory (as discussed in Appendix B), we still get an effective Hamiltonian H_{eff} of the following form that has the same eigenstates as the IRHM.

$$H_{eff} = \sum_{i,j>i} \left[J_{xy} \left(\sum_k S_k^z \right) (S_i^x S_j^x + S_i^y S_j^y) \right] + \sum_i J_z \left(\sum_k S_k^z \right) S_i^z, \quad (25)$$

where J_{xy} and J_z are functions of the $S_{Total}^z (= \sum_k S_k^z)$ operator. It is the infinite range of the Heisenberg model that enables the eigenstates of the system to remain unchanged. Furthermore, the ground state can also remain unchanged (with $S_T = 0$ and $S_T^z = 0$) if the effect of the term $-C \sum_i S_i^z$ with $C > 0$ [such as the last term in Eq. (22)] is canceled by a magnetic field. Thus the set of linearly independent ground states form the lowest energy subspace that is immune to decoherence. Furthermore, our highly entangled RVB states constructed from these ground states [such as those given by Eq. (13) for four qubits and by Eqs. (16)–(17) for six qubits] are also free of decoherence. Next, we study the decoherence in a dynamical context also and see how such ground states can remain robust and constitute a decoherence free subspace.

B. Dynamical evolution and DFS

The robustness of entanglement in a system can also be looked from the dynamical perspective. We consider

the following total Hamiltonian where all qubits of our IRHM interact identically with the environment.

$$H_{Tot} = H_{\text{IRHM}} + \sum_i S_i^z \sum_k g_k \omega_k (a_k^{\dagger} + a_k) + \sum_k \omega_k a_k^{\dagger} a_k. \quad (26)$$

The dynamics of the system can be studied through the following non-Markovian master equation for the reduced density operator $\rho_S(t)$ [44]:

$$\frac{d\rho_S(t)}{dt} = -i[H_S, \rho_S(t)] + F(t)[L\rho_S(t), L] + F^*(t)[L, \rho_S(t)L], \quad (27)$$

where H_S is the Hamiltonian of the system and L is the system operator that couples with the bath and satisfies the constraint $[L, H_S] = 0$. For the total Hamiltonian in Eq. (26), $H_S = H_{\text{IRHM}}$ and $L = \sum_i S_i^z$. Also, $F(t) = \int_0^t \alpha(t-s) ds$ where $\alpha(t-s) = \eta(t-s) + i\nu(t-s)$ is the bath correlation function at temperature T with

$$\eta(t-s) = \sum_k |g_k|^2 \coth\left(\frac{\omega_k}{2k_B T}\right) \cos[\omega_k(t-s)],$$

$$\nu(t-s) = - \sum_k |g_k|^2 \sin[\omega_k(t-s)]. \quad (28)$$

The function $F(t)$ governs the non-Markovian dynamical features of the system.

Let $\{|n\rangle\}$ be the eigen basis in which both the operators L and H_S are simultaneously diagonalized. Upon solving the master equation explicitly we get [44]:

$$\rho_{mn}(t) = \langle n | \rho_S | m \rangle \exp(-i[(E_n - E_m)t + (l_n^2 - l_m^2)Y(t)]) \times \exp[-(l_n - l_m)^2 X(t)] \rho_{mn}(0), \quad (29)$$

where E_n and l_n are defined through $H_{\text{IRHM}}|n\rangle = E_n|n\rangle$ and $\sum_i S_i^z |n\rangle = l_n |n\rangle$. Furthermore, $X(t) \equiv \int_0^t F_R(s) ds$ and $Y(t) \equiv \int_0^t F_I(s) ds$ with $F_R(t) + iF_I(t) \equiv F(t)$. This implies that, when states $|m\rangle$ and $|n\rangle$ have the same total spin S_T and the same z-component of the total spin S_T^z (i.e., $E_n = E_m$ and $l_n = l_m$), the matrix elements $\rho_{mn}(t) = \rho_{mn}(0)$ and the states $|m\rangle$ and $|n\rangle$ belong to DFS. Furthermore, the density matrix for two qubits at sites i, j (obtained from the groundstates of our SU(2) symmetric IHRM Hamiltonian) exhibits time independence, that is, $\rho_{ij}(t) = \rho_{ij}(0)$ with its elements given by Eq. (3). This shows that the dynamics of the system has no effect on the entanglement of the ground state of the system which implies that these states are highly/maximally robust. Consequently, our high E_v^2 RVB states constructed from the ground states of our IRHM are also free of decoherence. In future, using the above framework, we will consider the interesting case of dynamical evolution and decoherence of a superposition of states with different l_n values.

V. CONCLUSIONS.

Although both spins in a two-spin singlet state $|\uparrow\downarrow\rangle - |\downarrow\uparrow\rangle$ are monogamous (i.e., they cannot be entangled with any other spin), by using a homogenized superposition of valence bond states (each of which is a product of $N/2$ two-spin singlets), we managed to distribute entanglement efficiently such that any pair is maximally entangled with the rest of the RVB system while concomitantly the constituent spins of the pair are completely unentangled with each other. Thus we get the converse of monogamy for a pair of spins! Now, while total spin zero states are quite commonly ground states (as shown by Lieb-Mattis theorem [45]), it has not been recognized that one can generate high bipartite E_v^2 entanglement from such states. Our maximal E_v^2 RVB states are physically realizable in systems such as infinite-range large U/t Hubbard model and infinite-range hard-core boson model with frustrated hopping [46] when they are at half-filling.

Our high E_v^2 entanglement RVB states are free of decoherence when the system interacts locally with optical phonons. Furthermore, the set of orthogonal ground states of our IRHM form a DFS and evolve unitarily when all qubits are exposed to the same decohering collective noise. Thus our maximal E_v^2 RVB states are free of decoherence for two extreme types of coupling with the environment! Our decoherence free RVB states can be used for error free quantum computation and quantum communication.

In summary, our maximal E_v^2 RVB states have led us to IRHM for their realization and IRHM in turn generated maximal E_v^2 states as highly robust ground states.

Appendix A: Existence of homogeneous states for $N(\geq 8)$ qubit systems

Let $|\psi_n\rangle$ be a set of linearly independent $S_T = 0$ states with number of linearly independent states $n_L = \frac{N!}{(N/2)!(N/2+1)!}$. Then the homogeneous ground state can be written as:

$$|\Psi_{HGS}\rangle = \sum_{n=1}^{n_L} (\alpha_n + i\beta_n) |\psi_n\rangle \quad (\text{A1})$$

where α_n and β_n are real. We have ${}^N C_2$ number of $\langle S_i^z S_j^z \rangle$ correlation functions appearing in the expression for E_v^2 . For $N \geq 8$, we note that ${}^N C_2 \leq 2n_L$; in fact, the ratio $2n_L/{}^N C_2$ is unity for $N = 8$ while for $N > 8$ the ratio monotonically and rapidly increases. In order to maximize the system E_v^2 , we must have $\langle S_i^z S_j^z \rangle$ independent of i and j and thus make the system homogeneous. Homogeneity condition implies that the equality of the ${}^N C_2$ correlation functions $\langle S_i^z S_j^z \rangle$ produces ${}^N C_2 - 1$ independent equations. Now, in $|\Psi_{HGS}\rangle$, there are only $2n_L - 1$ independent α_n and β_n because of the normalization constraint. Furthermore for $N \geq 8$, in the ${}^N C_2 - 1$

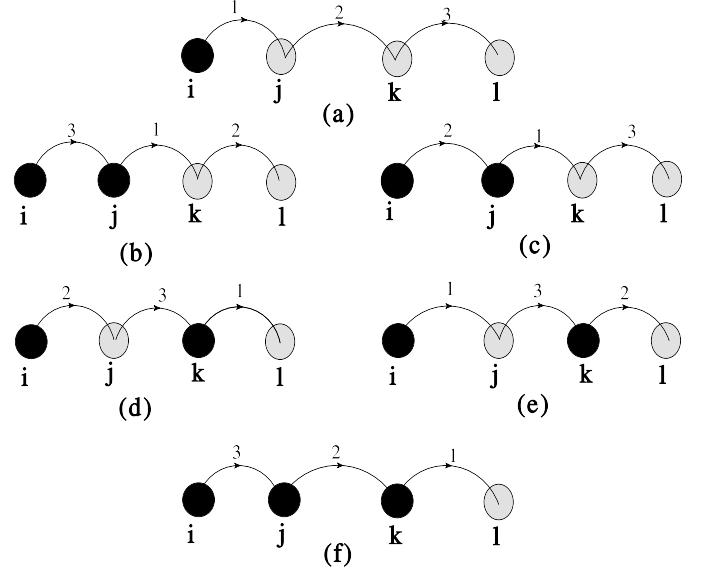


FIG. 3. Open loop hopping processes contributing to effective hopping term T_n^{li} in third-order perturbation theory. Here empty circles correspond to sites with no particles while filled circles correspond to sites with hard-core-bosons. The numbers 1, 2, and 3 indicate the order of hopping.

equations involving $\langle S_i^z S_j^z \rangle$, the number of independent coefficients is greater than or equal the number of equations, i.e., $2n_L - 1 \geq {}^N C_2 - 1$. Thus there are enough number of unknowns to produce homogeneity.

Appendix B: Third-order perturbation for IRHM system coupled to local phonons

The total Hamiltonian H_T , involving interaction with local optical phonons, is given by

$$H_T = H_{\text{IRHM}} + g\omega_0 \sum_i S_i^z (a_i^\dagger + a_i) + \omega_0 \sum_i a_i^\dagger a_i, \quad (\text{B1})$$

where a is the phonon destruction operator, ω_0 is the optical phonon frequency, and g is the coupling strength. Now, we make the connection that the spin operators can be expressed in terms of hard-core-boson (HCB) creation and destruction operators b^\dagger and b , i.e., $b^\dagger = S^+$, $b = S^-$, and $b^\dagger b = S^z + 0.5$. We then observe that conservation of S_{Total}^z implies conservation of total number of HCB. The total Hamiltonian is then given by

$$H = J \sum_{i,j>i} [0.5b_i^\dagger b_j + \text{H.c.} + n_i n_j] + \omega_0 \sum_j a_j^\dagger a_j + g\omega_0 \sum_j n_j (a_j + a_j^\dagger), \quad (\text{B2})$$

where $n_j \equiv b_j^\dagger b_j$. Then we perform the well-known Lang-Firsov (LF) transformation [47, 48] on this Hamiltonian. Under the LF transformation given by $e^S H e^{-S} =$

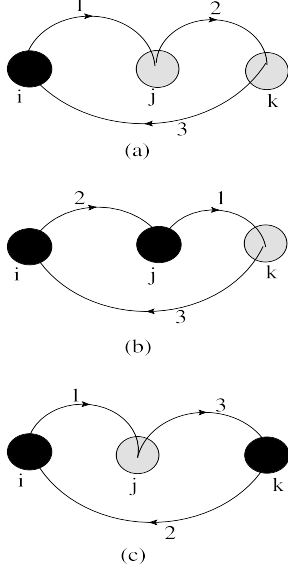


FIG. 4. Closed-loop hopping processes contributing to effective interaction term V_n^i in third-order perturbation theory. Here filled (empty) circles correspond to sites with (without) hard-core-bosons. The numbers 1, 2, and 3 represent hopping sequence.

$H_0 + H_1$ with $S = -g \sum_i n_i (a_i - a_i^\dagger)$, the operators b_j and a_j transform like fermions and phonons in the Holstein model. This is due to the interesting commutation properties of HCB given below:

$$\begin{aligned} [b_i, b_j] &= [b_i, b_j^\dagger] = 0, \text{ for } i \neq j, \\ \{b_i, b_i^\dagger\} &= 1. \end{aligned} \quad (\text{B3})$$

Next, the unperturbed Hamiltonian H_0 is identified to be [48]

$$\begin{aligned} H_0 &= J \sum_{i,j>i} [(0.5e^{-g^2} b_i^\dagger b_j + \text{H.c.}) + n_i n_j] \\ &+ \omega_0 \sum_j a_j^\dagger a_j - g^2 \omega_0 \sum_j n_j, \end{aligned} \quad (\text{B4})$$

while the perturbation H_1 is given by

$$H_1 = J \sum_{i,j>i} [0.5e^{-g^2} b_i^\dagger b_j + \text{H.c.}] \{ \mathcal{S}_+^{ij\dagger} \mathcal{S}_-^{ij} - 1 \}, \quad (\text{B5})$$

where $\mathcal{S}_\pm^{ij} = \exp[\pm g(a_i - a_j)]$ and $g^2 \omega_0$ is the polaronic binding energy.

Since the unperturbed Hamiltonian H_0 does not contain any interaction terms, we represent its eigenstates as $|n, m\rangle \equiv |n\rangle_{hcb} \otimes |m\rangle_{ph}$ with the corresponding eigenenergies $E_{n,m} = E_n^{hcb} + E_m^{ph}$. On observing that $\langle 0, 0 | H_1 | 0, 0 \rangle = 0$, we obtain the next relevant second-order perturbation term [48]

$$E^{(2)} = \sum_{n,m} \frac{\langle 0, 0 | H_1 | n, m \rangle \langle n, m | H_1 | 0, 0 \rangle}{E_{0,0} - E_{n,m}}. \quad (\text{B6})$$

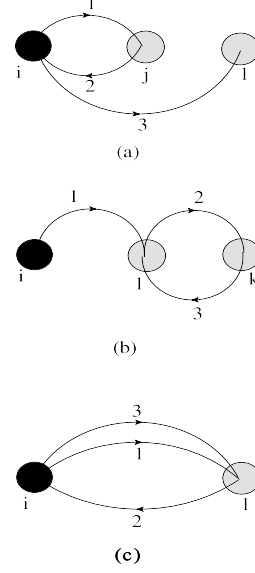


FIG. 5. Hopping processes (involving closed loops) contributing to effective hopping term T_{Cn}^{li} in third-order perturbation theory. Filled (empty) circles represent occupied (unoccupied) sites.

For strong coupling ($g > 1$) and non-adiabatic ($J/\omega_0 \leq 1$) conditions, on noting that $E_m^{ph} - E_0^{ph}$ is a positive integral multiple of ω_0 and $E_n^{hcb} - E_0^{hcb} \sim J e^{-g^2} \ll \omega_0$, we get the following second-order term [49]

$$H^{(2)} = \sum_{i,j>i} \left[(0.5J_\perp^{(2)} b_i^\dagger b_j + \text{H.c.}) + J_\parallel^{(2)} n_i n_j \right], \quad (\text{B7})$$

where

$$J_\perp^{(2)} \equiv -(N-2) f_1(g) \frac{J^2 e^{-2g^2}}{2\omega_0} \sim -(N-2) \frac{J^2 e^{-g^2}}{2g^2 \omega_0}, \quad (\text{B8})$$

$$J_\parallel^{(2)} \equiv [2f_1(g) + f_2(g)] \frac{J^2 e^{-2g^2}}{2\omega_0} \sim \frac{J^2}{4g^2 \omega_0}, \quad (\text{B9})$$

with $f_1(g) \equiv \sum_{n=1}^{\infty} g^{2n}/(n!n)$ and $f_2(g) \equiv \sum_{n=1}^{\infty} \sum_{m=1}^{\infty} g^{2(n+m)}/[n!m!(n+m)]$. The small parameter for our perturbation theory is $t/(g\omega_0)$. We now make the important observation that the eigenstates of the effective Hamiltonian $H_0 + H^{(2)}$ are identical to those of the original Hamiltonian H_{IRHM} in Eq. (10) because $\sum_{i,j>i} (S_i^z S_j^z)$ and H_{IRHM} commute.

Next, we will show that the third-order perturbation theory also produces a term that has the same eigenstates as IRHM. To this end, we obtain the following third-order perturbation term in the effective Hamiltonian:

$$H^{(3)} = \sum_{m \neq 0, n \neq 0} \frac{\langle 0|H_1|m\rangle_{ph} \langle m|H_1|n\rangle_{ph} \langle n|H_1|0\rangle_{ph}}{\Delta E_m \Delta E_n}. \quad (\text{B10})$$

Here $\Delta E_m = E_m^{ph} - E_0^{ph}$. Evaluation of $H^{(3)}$ leads to various hopping terms and interaction terms.

$$H^{(3)} = \sum_{i, l \neq i} \left[\sum_{n=1}^6 t_n T_n^{li} + \sum_{n=1}^3 t_{cn} T_{Cn}^{li} \right] + \sum_i \sum_{n=1}^3 v_n V_n^i, \quad (\text{B11})$$

where $t_n \sim (J^3 e^{-g^2}) / (g^2 \omega_0)^2$, $t_{cn} \sim J^3 e^{-g^2} / (g \omega_0)^2$, and $v_n \sim J^3 / (g^2 \omega_0)^2$ (as will be explained later). We will demonstrate below that $H^{(3)}$ is of the following form

$$H^{(3)} = \sum_{i, l > i} \left[T \left(\sum_k n_k \right) b_l^\dagger b_i + \text{H.c.} \right] + \sum_i V \left(\sum_k n_k \right) n_i. \quad (\text{B12})$$

where T and V are functions of the total number operator $\sum_k n_k$. Since the IRHM commutes with the total number operator, $H^{(3)}$ has the same eigenstates as IRHM!

There are six open-loop hopping processes T_n^{li} depicted in Fig. 3. We analyze them sequentially below.

$$\begin{aligned} T_1^{li} &= \sum_{k \neq i, l, j} \sum_{j \neq i, l} b_l^\dagger b_k b_k^\dagger b_j b_j^\dagger b_i \\ &= \sum_{k \neq i, l, j} (1 - b_k^\dagger b_k) \sum_{j \neq i, l} (1 - b_j^\dagger b_j) b_l^\dagger b_i \\ &= \left[\sum_{k \neq i, l} (1 - b_k^\dagger b_k) - 1 \right] \left[\sum_{j \neq i, l} (1 - b_j^\dagger b_j) \right] b_l^\dagger b_i \\ &= \left[\sum_{k \neq i, l} (1 - b_k^\dagger b_k) - 1 \right] \left[(N - 2) - \sum_{j \neq l} b_j^\dagger b_j \right] b_l^\dagger b_i \\ &= \left[\sum_{k \neq i, l} (1 - b_k^\dagger b_k) - 1 \right] \left[(N - 1) - \sum_j b_j^\dagger b_j \right] b_l^\dagger b_i \\ &= \left[(N - 1) - \sum_j b_j^\dagger b_j \right] \left[\sum_{k \neq i, l} (1 - b_k^\dagger b_k) - 1 \right] b_l^\dagger b_i \\ &= \left[(N - 1) - \sum_j b_j^\dagger b_j \right] \left[(N - 2) - \sum_k b_k^\dagger b_k \right] b_l^\dagger b_i. \end{aligned} \quad (\text{B13})$$

The second hopping process T_2^{li} in Fig. 3 (b) is given by

$$\begin{aligned} T_2^{li} &= \sum_{k \neq i, l, j} \sum_{j \neq i, l} b_j^\dagger b_i b_l^\dagger b_k b_k^\dagger b_j \\ &= \sum_{k \neq i, l, j} (1 - b_k^\dagger b_k) \sum_{j \neq i, l} b_j^\dagger b_j b_l^\dagger b_i \\ &= \sum_{k \neq i, l} (1 - b_k^\dagger b_k) \sum_{j \neq i, l} b_j^\dagger b_j b_l^\dagger b_i \\ &= \sum_{k \neq i, l} (1 - b_k^\dagger b_k) \left[\sum_j b_j^\dagger b_j - 1 \right] b_l^\dagger b_i \\ &= \left[\sum_j b_j^\dagger b_j - 1 \right] \left[(N - 1) - \sum_k b_k^\dagger b_k \right] b_l^\dagger b_i. \end{aligned} \quad (\text{B14})$$

The hopping process T_3^{li} in Fig. 3 (c) is expressed as $T_3^{li} = \sum_{k \neq i, l, j} \sum_{j \neq i, l} b_l^\dagger b_k b_j^\dagger b_i b_k^\dagger b_j = T_2^{li}$. The fourth hopping process T_4^{li} in Fig. 3 (d) is obtained as follows.

$$\begin{aligned} T_4^{li} &= \sum_{j \neq i, l, k} \sum_{k \neq i, l} b_k^\dagger b_j b_j^\dagger b_i b_l^\dagger b_k \\ &= \sum_{j \neq i, l, k} (1 - b_j^\dagger b_j) \sum_{k \neq i, l} b_k^\dagger b_k b_l^\dagger b_i \\ &= T_2^{li}. \end{aligned} \quad (\text{B15})$$

The hopping process T_5^{li} in Fig. 3 (e) yields $T_5^{li} = \sum_{j \neq i, l, k} \sum_{k \neq i, l} b_k^\dagger b_j b_l^\dagger b_k b_j^\dagger b_i = T_4^{li}$. We analyze below the last hopping process T_6^{li} in Fig. 3 (f).

$$\begin{aligned} T_6^{li} &= \sum_{k \neq i, l, j} \sum_{j \neq i, l} b_j^\dagger b_i b_k^\dagger b_l b_l^\dagger b_k \\ &= \sum_{k \neq i, l, j} b_k^\dagger b_k \sum_{j \neq i, l} b_j^\dagger b_j b_l^\dagger b_i \\ &= \left[\sum_{k \neq i, l} b_k^\dagger b_k - 1 \right] \sum_{j \neq i, l} b_j^\dagger b_j b_l^\dagger b_i \\ &= \left[\sum_{k \neq i, l} b_k^\dagger b_k - 1 \right] \left[\sum_j b_j^\dagger b_j - 1 \right] b_l^\dagger b_i \\ &= \left[\sum_j b_j^\dagger b_j - 1 \right] \left[\sum_k b_k^\dagger b_k - 2 \right] b_l^\dagger b_i. \end{aligned} \quad (\text{B16})$$

We will now deal with closed-loop hopping processes such as those in Fig 4. These lead to effective interactions. The process V_1^i in Fig. 4 (a), obtained from Fig.

3 (a) by setting $l = i$, is given as follows.

$$\begin{aligned}
V_1^i &= \sum_{k \neq i, j} \sum_{j \neq i} b_i^\dagger b_k b_k^\dagger b_j b_j^\dagger b_i \\
&= \sum_{k \neq i, j} (1 - b_k^\dagger b_k) \sum_{j \neq i} (1 - b_j^\dagger b_j) b_i^\dagger b_i \\
&= \left[\sum_{k \neq i} (1 - b_k^\dagger b_k) - 1 \right] \left[\sum_{j \neq i} (1 - b_j^\dagger b_j) \right] b_i^\dagger b_i \\
&= \left[(N) - \sum_j b_j^\dagger b_j \right] \left[(N - 1) - \sum_k b_k^\dagger b_k \right] b_i^\dagger b_i \quad (\text{B17})
\end{aligned}$$

Next, the hopping process V_2^i corresponding to closed loop in Fig. 4 (b) is obtained from Fig. 3 (c) by taking $l = i$.

$$\begin{aligned}
V_2^i &= \sum_{k \neq i, j} \sum_{j \neq i} b_i^\dagger b_k b_j^\dagger b_i b_k^\dagger b_j \\
&= \sum_{k \neq i, j} (1 - b_k^\dagger b_k) \sum_{j \neq i} b_j^\dagger b_j b_i^\dagger b_i \\
&= \sum_{k \neq i} (1 - b_k^\dagger b_k) \sum_{j \neq i} b_j^\dagger b_j b_i^\dagger b_i \\
&= \sum_{k \neq i} (1 - b_k^\dagger b_k) \left[\sum_j b_j^\dagger b_j - 1 \right] b_i^\dagger b_i \\
&= \left[\sum_j b_j^\dagger b_j - 1 \right] \left[(N) - \sum_k b_k^\dagger b_k \right] b_i^\dagger b_i. \quad (\text{B18})
\end{aligned}$$

Lastly, the hopping V_3^i [depicted by the closed loop in Fig. 4 (c)] is obtained from Fig. 3 (e) by setting $l = i$.

$$\begin{aligned}
V_3^i &= \sum_{j \neq i, k} \sum_{k \neq i} b_k^\dagger b_j b_i^\dagger b_k b_j^\dagger b_i \\
&= \sum_{j \neq i, k} (1 - b_j^\dagger b_j) \sum_{k \neq i} b_k^\dagger b_k b_i^\dagger b_i \\
&= V_2^i. \quad (\text{B19})
\end{aligned}$$

Finally, we consider Figs. 5 (a), (b), and (c) which deal with effective hopping terms $T_{C_n}^{li}$ involving closed loops. The effective hopping term $T_{C_1}^{li}$, corresponding to Fig. 5 (a), is obtained by setting $k = i$ in Fig. 3 (a):

$$\begin{aligned}
T_{C_1}^{li} &= \sum_{j \neq i, l} b_l^\dagger b_i b_i^\dagger b_j b_j^\dagger b_i \\
&= \sum_{j \neq i, l} (1 - b_j^\dagger b_j) b_l^\dagger b_i \\
&= \left[(N - 2) - \sum_{j \neq l} b_j^\dagger b_j \right] b_l^\dagger b_i \\
&= \left[(N - 1) - \sum_j b_j^\dagger b_j \right] b_l^\dagger b_i. \quad (\text{B20})
\end{aligned}$$

To obtain the effective hopping term $T_{C_2}^{li}$ corresponding to Fig. 5 (b), we take $j = l$ in Fig. 3 (a):

$$\begin{aligned}
T_{C_2}^{li} &= \sum_{k \neq i, l} b_l^\dagger b_k b_k^\dagger b_l b_l^\dagger b_i \\
&= \sum_{k \neq i, l} (1 - b_k^\dagger b_k) b_l^\dagger b_i \\
&= \left[(N - 2) - \sum_{k \neq l} b_k^\dagger b_k \right] b_l^\dagger b_i \\
&= \left[(N - 1) - \sum_k b_k^\dagger b_k \right] b_l^\dagger b_i \\
&= T_{C_1}^{li}. \quad (\text{B21})
\end{aligned}$$

The effective hopping term $T_{C_3}^{li}$ depicted in Fig. 5 (c) [upon setting $k = i$ and $j = l$ in Fig. 3 (a)] is given by

$$T_{C_3}^{li} = b_l^\dagger b_i b_i^\dagger b_l b_l^\dagger b_i = b_l^\dagger b_i. \quad (\text{B22})$$

Thus we have shown that $H^{(3)}$ contains effective hopping terms ($\sum_{i, l > i} [T(\sum_k n_k) b_l^\dagger b_i + \text{H.c.}]$) and effective interaction terms ($\sum_i V(\sum_k n_k) n_i$). Since T and V are functions of the total number operator, $H^{(3)}$ and IRHM have the same eigenstates. These arguments can be extended to even higher-order perturbation theory to show that the effective Hamiltonian (after taking all orders of perturbation into account) will give the same eigenstates as IRHM!

We will now explain the expressions for the coefficients t_n , v_n , and t_{cn} in Eq. (B11), obtained from third-order perturbation theory, using typical schematic diagrams shown in Fig. 6 [50]. We consider two distinct time scales associated with hopping processes between two sites: (i) $\sim 1/(J e^{-g^2})$ corresponding to either full distortion at a site to form a small polaronic potential well (of energy $-g^2 \omega_0$) or full relaxation from the small polaronic distortion and (ii) $\sim 1/J$ related to negligible distortion/relaxation at a site. The coefficient t_n corresponds to the typical dominant distortion processes shown schematically in Fig. 6 (a) with the pertinent typical hopping processes being depicted in Fig. 3 (a). In Fig. 6 (a), after the HCB hops away from the initial site, the intermediate states have the same distortion as the initial state. Next, when the HCB hops to its final site there is a distortion at this final site with a concomitant relaxation at the initial site. Hence the contribution to the coefficient t_n becomes $J/(2g^2 \omega_0) \times J/(2g^2 \omega_0) \times J e^{-g^2} \sim J^3 e^{-g^2} / (g^2 \omega_0)^2$. As regards coefficient v_n , it can be deduced based on the typical dominant hopping-cum-distortion processes depicted in Fig. 6 (b) which typifies the hopping processes in Fig. 4 (a). In Fig. 6 (b), when the particle hops to different sites and reaches finally the initial site, there is no change in distortion at any site. Hence V_n can be estimated to be $J/(2g^2 \omega_0) \times J/(2g^2 \omega_0) \times J \sim J^3 / (g^2 \omega_0)^2$. Lastly, we obtain the coefficient t_{cn} by considering the typical dominant diagram in Fig. 6 (c) corresponding to the typical

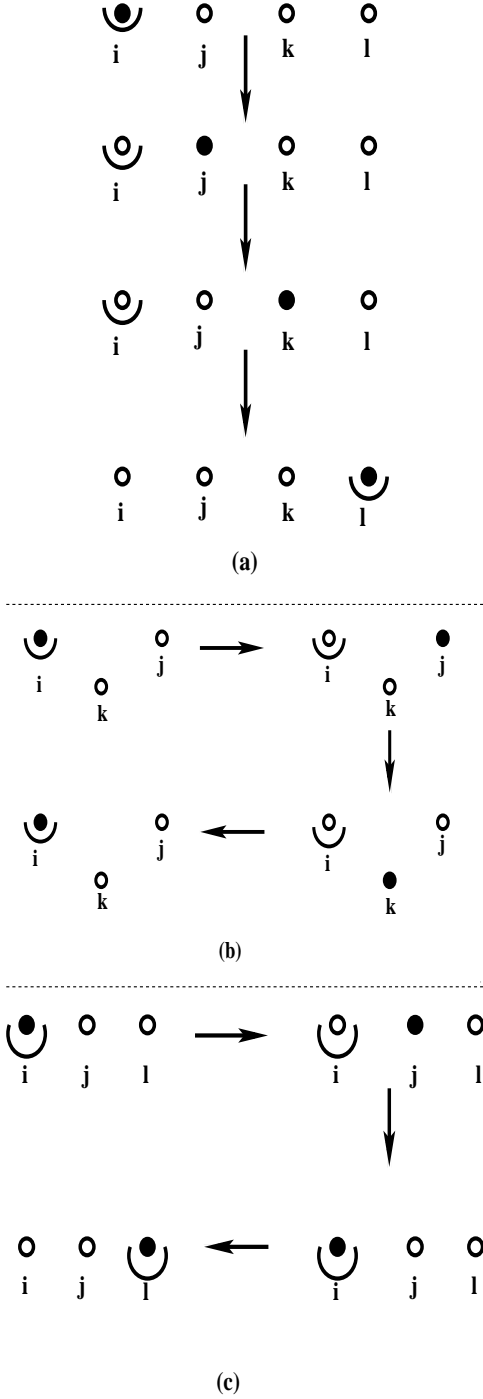


FIG. 6. Schematic diagrams (a), (b), and (c), corresponding to the hopping processes depicted in Fig. 3 (a), Fig. 4 (a), and Fig. 5 (a) respectively, yield coefficients t_n , v_n , and t_{cn} respectively. The intermediate states give the typical dominant contributions. Here empty circles correspond to empty sites, while filled circles indicate particle positions. Parabolic curve at a site depicts full distortion at that site with corresponding energy $-g^2\omega_0$ ($+g^2\omega_0$) if the hard-core-boson is present (absent) at that site.

process in Fig. 5 (a). In Fig. 6 (c), where the first intermediate state depicts the particle hopping but leaving the distortion unchanged, we get a contribution $J/(2g^2\omega_0)$; for the next intermediate state, where the HCB returns to the initial site, the initial site has to undergo a slight relaxation (involving absorbing a phonon so as to yield a non-zero denominator in the perturbation theory) leading to the contribution J/ω_0 ; and lastly, when the HCB hops to the final site, there is a distortion at the final site with a simultaneous relaxation at the initial site thereby producing a contribution Je^{-g^2} . Thus we calculate v_n to be $J/(2g^2\omega_0) \times J/\omega_0 \times Je^{-g^2} \sim J^3 e^{-g^2}/(g\omega_0)^2$ [51].

-
- [1] M. A. Nielsen and I. Chuang, *Quantum Computation and Quantum Communication* (Cambridge University Press, Cambridge, 2000).
- [2] G. Vidal, Phys. Rev. Lett. **91**, 147902 (2003).
- [3] J. I. Latorre and A. Riera, J. Phys. A: Math. Theor. **42**, 504002 (2009).
- [4] R. Horodecki, P. Horodecki, M. Horodecki, and K. Horodecki, Rev. Mod. Phys. **81**, 865 (2009).
- [5] M. B. Plenio and S. Virmani, Quant. Inf. Comp. **7**, 1 (2007).
- [6] D. A. Meyer and N. R. Wallach J. Math. Phys, **43** , 4273 (2002).
- [7] A. J. Scott Phys. Rev. A, **69**, 052330 (2004).
- [8] A. R. R. Carvalho, F. Mintert, and A. Buchleitner, Phys. Rev. Lett, **93**, 230501 (2004).
- [9] P. Facchi, G. Florio, and S. Pascazio, Phys. Rev. A **74**, 042331 (2006).
- [10] A. Borrás, A. R. Plastino, J. Batle, C. Zander, M. Casas, and A. Plastino, J. Phys. A: Math. Theor. **40**, 13407 (2007).
- [11] G. Adesso and F. Illuminati, Phys. Rev. Lett, **99**, 150501 (2007).
- [12] P. Facchi, G. Florio, G. Parisi, and S. Pascazio, Phys. Rev. A **77**, 060304(R) (2008).
- [13] I. D. K. Brown, S. Stepney, A. Sudbery, and S. L. Braunstein, J. Phys. A: Math. Gen. **38**, 1119 (2005).
- [14] A. Higuchi and A. Sudbery, Phys. Lett. A **273**, 213 (2000).
- [15] B. Rothlisberger, J. Lehmann, D. S. Saraga, P. Traber, and D. Loss, Phys. Rev. Lett. **100**, 100502 (2008).
- [16] P. Facchi, G. Florio, S. Pascazio, and F. Pepe, Phys. Rev. A **82**, 042313 (2010).
- [17] M. Schlosshauer, Rev. Mod. Phys. **76**, 1267 (2005).
- [18] G. M. Palma, K. Suominen, and A. K. Ekert, Proc. R. Soc. London, Ser. A **452**, 567 (1996); L.-M. Duan and G.-C. Guo, Phys. Rev. A **57**, 737 (1998).
- [19] P. Zanardi and M. Rasetti, Phys. Rev. Lett. **79**, 3306 (1997).
- [20] D. A. Lidar, I. L. Chuang, and K. B. Whaley, Phys. Rev. Lett. **81**, 2594 (1998).
- [21] J. Kempe, D. Bacon, D. A. Lidar, and K. B. Whaley, Phys. Rev. A **63**, 042307 (2001).
- [22] J.-C. Boileau, D. Gottesman, R. Laflamme, D. Poulin, and R. W. Spekkens, Phys. Rev. Lett. **92**, 017901 (2004).
- [23] T.-Y. Chen, J. Zhang, J.-C. Boileau, X.-M. Jin, B. Yang, Q. Zhang, T. Yang, R. Laflamme, and J.-W. Pan, Phys. Rev. Lett. **96**, 150504 (2006).
- [24] S. D. Bartlett, T. Rudolph, and R. W. Spekkens, Phys. Rev. Lett. **91**, 027901 (2003).
- [25] A. Cabello, Phys. Rev. A **68**, 042104 (2003).
- [26] A. Cabello, Phys. Rev. A **75**, 020301 (2007).
- [27] P. W. Anderson, Science **235**, 1196 (1987).
- [28] P. A. Lee, N. Nagaosa, and X.-G. Wen, Rev. Mod. Phys. **78**, 17 (2006).
- [29] T. Ishiguro, K. Yamaji, and G. Saito, Organic Superconductors (Springer, New York, 1998).
- [30] E. A. Ekimov, V. A. Sidorov, E. D. Bauer, N. N. Mel'nik, N. J. Curro, J. D. Thompson, and S. M. Stishov, Nature (London) **428**, 542 (2004).
- [31] A. Y. Kitaev, Ann. Phys. (N.Y.) **303**, 2 (2003).
- [32] S. Liang and P. W. Anderson, Phys. Rev. Lett. **61**, 365 (1998).
- [33] A. Chandran, D. Kaszlikowski, A. Sen(De), U. Sen and V. Vedral, Phys. Rev. Lett. **99**, 170502 (2007); D. Kaszlikowski, Aditi Sen(De), Ujjwal Sen, and V. Vedral, Phys. Rev. Lett. **101**, 248902 (2008); F. Alet, D. Braun, and G. Misguich, Phys. Rev. Lett. **101**, 248901 (2008).
- [34] F. Alet, S. Capponi, N. Laflorencie, and M. Mambrini, Phys. Rev. Lett. **99**, 117204 (2007).
- [35] U. Glaser, H. Büttner, and H. Fehske, Phys. Rev. A. **68**, 032318 (2003).
- [36] P. Rungta, V. Bužek, Carlton M. Caves, M. Hillery, and G. J. Milburn, Phys. Rev. A **64**, 042315 (2001).
- [37] Chanchal K. Majumdar and Dipan K. Ghosh, J. Math. Phys. **10**, 1388 (1969).
- [38] G. Rumer, Nachr. d. Ges. d. Wiss. zu Göttingen, M. P. Klasse, 337 (1932).
- [39] L. Pauling, J. Chem. Phys. **1**, 280 (1933).
- [40] S.-J. Gu, H. Li, Y.-Q. Li, and H.-Q. Lin, Phys. Rev. A **70**, 052302 (2004).
- [41] I. Bose and A. Tribedi, Phys. Rev. A **72**, 022314 (2005).
- [42] A. Cabello, J. Mod. Opt. **50**, 10049 (2003).
- [43] In Ref. 33 it was pointed out that the “RVB liquid” on a 4×4 square lattice gives $p > 1/3$ for periodic boundary conditions while it yields $p < 1/3$ in the interior of a sample with open boundary conditions.
- [44] T. Yu and J.H. Eberly, Phys. Rev. B **66**, 193306 (2002).
- [45] E. Lieb and D. Mattis, Phys. Rev. **125**, 164 (1962).
- [46] For examples of frustrated hopping, see F. Wang, F. Pollmann, and A. Vishwanath, Phys. Rev. Lett. **102**, 017203 (2009).
- [47] I.G. Lang and Yu.A. Firsov, Zh. Eksp. Teor. Fiz. **43**, 1843 (1962). [Sov. Phys. JETP **16**, 1301 (1962)].
- [48] S. Datta, A. Das, and S. Yarlagadda, Phys. Rev. B **71**, 235118 (2005).
- [49] S. Datta and S. Yarlagadda, Solid State Commun. **150**, 2040 (2010).
- [50] Detailed analysis has been carried out for second-order perturbation theory in Sahinur Reja, Sudhakar Yarlagadda, and Peter B. Littlewood, Phys. Rev. B **84**, 085127 (2011).
- [51] S. Yarlagadda, e-print arXiv:0712.0366v2.